Large Eddy Simulation of Supercritical Mixing Layers

M. Jarczyk⋆, M. Pfitzner⋆, C. A. Niedermeier⋆⋆, S. Hickel⋆⋆ and N. A. Adams⋆⋆
⋆Institute for Thermodynamics, Universität der Bundeswehr München
Werner-Heisenberg-Weg 39, 85577 Neubiberg, Germany
⋆⋆Institute of Aerodynamics and Fluid Mechanics, Technische Universität München
Boltzmannstraße 15, 85748 Garching bei München, Germany

Abstract

Within the development of a validated and reliable numerical tool for the simulation of a whole rocket combustion chamber, real gas thermodynamics has been implemented into two CFD codes, an in-house code and OpenFOAM. The presented work is part of the validation process, where different LES simulations were conducted with these codes. The implicit LES method ALDM and two explicit one equation models - dynamic and non-dynamic - were validated against DNS simulations of a non-reacting transient mixing layer. Both codes reproduced the DNS data very well. A future task will be the optimization of the LES models for real gas flows and subsequent combustion simulations.

1. Introduction

The technology of cryogenic rocket combustion engines has been used successfully for many years and is well known today. Nowadays, a new challenge is the requirement of increasing rocket performance and reliability at even more restricted budgets and shortened development cycles. For this reason, the application of computational methods in the development process increases steadily and therefore also the demand for computational fluid dynamics (CFD) tools which are able to simulate the flow at rocket combustor conditions. The pressure in modern combustion chambers often exceeds 10 MPa, causing many propellants, like oxygen and hydrogen, to become supercritical at injection. In this high pressure environment molecular interactions significantly affect the fluid properties. Hence, a real gas equation of state and suitable relations for the transport properties have to be used for the numerical simulation. We apply the cubic Peng-Robinson (PR) [1] equation of state (EOS) combined with an empirical volume correction method to obtain the thermodynamic behaviour of the real gas [2]. The ultimate goal of our work is to analyze the propellant injection into a rocket combustion chamber through multiple coaxial injectors and the subsequent combustion process. As this process is strongly three-dimensional and unsteady, Large Eddy Simulation (LES) is the most promising method to gain deeper insight into the relevant physical processes. As a first step towards this goal, a non-reacting, transitional, temporal mixing layer of hydrogen and oxygen studied by Okong'o et al. [3] is used in the present work as test case for validating the two CFD codes. The Institute for Thermodynamics of the Universität der Bundeswehr München uses the multi-component solver of the OpenFOAM package with an explicit one equation model (dynamic (DOEM) and non-dynamic (OEM)) as subgrid-scale (SGS) model, whereas the simulations carried out at the Institute of Aerodynamics and Fluid Mechanics at the Technische Universität München (TUM) are conducted by means of an in-house CFD code (INCA) using an implicit LES (ILES) method, namely the Adaptive Local Deconvolution Method (ALDM). This method was successfully validated for compressible flows of ideal gases ([4] and [5]) and its usage is now extended to real gas flows. Additionally, Direct Numerical Simulations (DNS) are conducted with this code to have an own reference database for comparison with the LES results. The paper is organized as follows: In Sec. 2, the underlying conservation equations which are solved by our codes are briefly depicted. Secs. 3 and 4 describe the SGS and thermodynamic modeling approaches, while in Secs. 5 and 6 the transport coefficients and the boundary and initial conditions of the simulations are given. The results for the evolution of global mixing layer quantities as well as flow visualizations of different variables at the transitional time are shown in Sec. 7. In Sec. 8, we draw conclusions from our results and give an outlook to future work.

2. Conservation Equations

The general conservations equations for the H_2/O_2 binary mixture under consideration are given by Okong'o et al. [3] as

$$\frac{\partial \rho}{\partial t} + \frac{\partial \left(\rho u_j\right)}{\partial x_j} = 0 \tag{1}$$

$$\frac{\partial \left(\rho u_i\right)}{\partial t} + \frac{\partial \left(\rho u_i u_j + p\delta_{ij}\right)}{\partial x_j} = \frac{\partial \tau_{ij}}{\partial x_j} \tag{2}$$

$$\frac{\partial \rho Y_O}{\partial t} + \frac{\partial \left(\rho Y_O u_j\right)}{\partial x_j} = -\frac{\partial j_{Oj}}{\partial x_j} \tag{3}$$

$$\frac{\partial \rho e_t}{\partial t} + \frac{\partial \left[\left(\rho e_t + p\right) u_j\right]}{\partial x_j} = -\frac{\partial q_{IKj}}{\partial x_j} + \frac{\partial \tau_{ij} u_i}{\partial x_j} \tag{4}$$

Here x_j are cartesian coordinates, t is the time, ρ is the density, u_i is the velocity component in direction i, $e_t = e + u_i u_i/2$ is the total energy, p is the thermodynamic pressure and Y_O is the oxygen mass fraction. q_{IKj} is the Irwing-Kirkwood (IK) form of the heat flux vector [6], j_{Oi} is the oxygen mass flux in direction i and τ_{ij} is the Newtonian viscous stress tensor. A detailed description of the flux calculation can be found in [3] and [7]. This flux formulation includes Dufour and Soret effect as well as diffusion due to pressure gradients. In the investigated test case this very detailed diffusion modelling is needed for a physical reproduction of the flow field.

The CFD codes follow two different approaches. The in-house code used for DNS and ILES is a density based code directly solving the set of equations given above (Eqns. (1) - (4)), whereas the OpenFOAM solver uses a pressure based PISO (Pressure Implicit with Splitting of Operators) algorithm proposed by Issa et al. ([8] and [9]).

The PISO algorithm for compressible flows used in OpenFOAM has been developed from an incompressible approach. As in the incompressible limit the continuity equation becomes an auxiliary condition more than a conservation equation, it is no longer reasonable to solve the system of equation above. Therefore pressure based algorithms have been developed, where a conservation equation for the pressure (developed from the discretised momentum and continuity equation) is solved in place of Eq. 1. A special issue is here the nonlinearity of the equation of state needed in high pressure environments, which has to be accounted for in the solution approach. Energy conservation in OpenFOAM is realised by solving an enthalpy equation (Eqn. (5)) instead of the total energy e_t equation (Eqn. (4)).

$$\frac{\partial \rho h}{\partial t} + \frac{\partial \left(\rho h u_j\right)}{\partial x_j} = -\frac{\partial q_{IKj}}{\partial x_j} + \frac{Dp}{Dt} \tag{5}$$

The viscous heating term $\partial \tau_{ij} u_i / \partial x_j$ is neglected here as it is known to negatively influence stability in pressure based solution approaches and as it is negligible in the low velocity flows studied here.

3. Turbulence Modelling and Numerics

As an intermediate approach between Reynolds-averaged Navier-Stokes (RANS) and DNS, LES resolves the large scales of turbulence while the small scales below the filtering width have to be modeled. When an explicit SGS model like the OEM is used, it is strongly coupled to the numerical scheme which is used to discretise the Navier-Stokes equations. Here the truncation error of the approximated convective terms has the same order of magnitude as the effects of the SGS model, since the smallest scales on which the SGS model operates are not fully resolved. Hence, the accuracy of the solution is influenced by this mutual interference, potentially affecing the prediction reliability.

Another possibility is to directly use the truncation error of the unmodified conservation equations as a physically motivated SGS model. This merging of numerical scheme and SGS model is called Implicit LES and both explicit LES (with OEM) and ILES (with ALDM) are used in the present work.

ALDM incorporates free parameters in the discretisation scheme which can be used to control the truncation error. These parameters are calibrated according to several common test cases, such as isotropic compressible turbulence [4], to have a physically meaningful SGS model. ALDM is implemented for Cartesian collocated grids and used to discretize the convective terms of the Navier-Stokes equations. The diffusive terms are dircretised by means of 2^{nd}

order centered differences while a 3^{rd} order explicit Runge-Kutta method is used for time integration. For the DNS conducted in the present work, the convective terms are also discretised by 2^{nd} order centered differences.

For explicit LES a compressible version of the OEM and DOEM is used in OpenFOAM [10]. In this model an additional transport equation for the turbulent kinetic energy is solved, which is then used to calculate the eddy viscosity. With OpenFOAM, 2^{nd} order centered differencing has been applied for spatial discretisation and a 2^{nd} order backward scheme has been used for time integration.

4. Thermodynamic Modelling

All thermodynamic properties are calculated as the sum of an ideal reference value and a departure function accounting for real gas effects which is calculated using a real gas equation of state. For closure of the system of conservation equations, enthalpy h and constant-pressure specific heat c_p (OpenFOAM) and accordingly internal energy e and constant-volume specific heat c_v (ALDM) have to be provided. These are defined the as

$$h(T,p) = h_0(T) + \int_{p_0}^{p} \left(V_m - T\left(\frac{\partial V_m}{\partial T}\right)_p \right) \mathrm{d}p \tag{6}$$

$$e(T,V) = e_0(T) + \int_{V}^{V_\infty} \left(p - T\left(\frac{\partial p}{\partial T}\right)_V \right) \mathrm{d}V \tag{7}$$

$$c_p(T,p) = c_v(T,p) - \frac{T\left(\frac{\partial p}{\partial T}\right)_V^2}{\left(\frac{\partial p}{\partial V}\right)_T} \tag{8}$$

$$c_v(T,V) = \left(\frac{\partial e}{\partial T}\right)_V \tag{9}$$

Here the subscript 0 refers to the ideal reference state at low pressure. The departure functions on the right hand side have to be determined using an appropriate equation of state. In the work presented here the Peng-Robinson (PR) equation (Eqn. (10)) has been applied.

$$p = \frac{RT}{V-b} - \frac{a(T)}{V^2 + 2Vb - b^2} \tag{10}$$

V is the molar volume and R is the universal gas constant with a value of $R = 8.314472$ J/molK. The constants $a(T)$ and b are calculated from empirical relations. $a(T)$ accounts for attractive forces between the molecules in the fluid and is calculated from the empirical equation (11).

$$a(T) = 0.457235 \frac{R^2 T_c^2}{p_c} \cdot \left(1 - \kappa \left(1 - \sqrt{\frac{T}{T_c}} \right) \right)^2 \tag{11}$$

$\kappa = 0.37464 + 1.54226\omega - 0.26992\omega^2$ is a function of the acentric factor ω. $b = 0.077796 RT_c/p_c$ takes into account the effects of the reduction of free volume by the particular volume of the molecules. T_c and p_c are the critical temperature and pressure of the modelled species (H_2: 33.2 K / 13 bar, O_2: 154.6 K / 50.4 bar). For multi-component mixtures, the extended corresponding states principle is applied, where a mixture of a fixed composition is assumed to behave like a pure fluid. The mixture properties are also calculated using the PR equation of state with parameters a and b calculated form real gas mixing rules (Eqns. (12) - (13)).

$$a = \sum_i \sum_j x_i x_j a_{ij} \tag{12}$$

$$b = \sum_i x_i b_i \tag{13}$$

Here a_i and b_i are the pure component parameters. a_{ij} is calculated from $a_{ij} = \sqrt{a_i a_j}(1 - k_{ij})$ with the binary interaction coefficient k_{ij}, which is set to zero for the investigations below. As the Peng-Robinson equation of state is known to be not very accurate in predicting the density in transcritical regions an empirical correction method established by Harstad et al. [2] has been chosen for the final implementation.

5. Transport Coefficients

We calculate the transport coefficients by using empirical correlations given by Okong'o et al. [3] (Eqs. (14) - (16)).

$$\mu = \mu_R \left(T / \left[0.5 \left(T_1 + T_2\right)\right]\right)^{0.75} \tag{14}$$

$$Sc = \mu / \left(\rho \alpha_D D\right) = \left(1.334 - 0.668 Y_O - 0.186 Y_O^2 - 0.268 Y_O^6\right) \times \left[1 + \left(88.6/T\right)^{1.5}\right] \tag{15}$$

$$Pr = \mu C_p / (m\lambda) = 1.335 / T^{0.1} \tag{16}$$

The Reynolds number Re of the mixing layer is adjusted using the reference viscosity μ_R which can be calculated from Eq. (17). The investigations presented in this work were carried out at $Re = 750$, a value which is sufficient for the mixing layer's transition [3].

$$Re = \frac{0.5 \left(\rho_1 + \rho_2\right) \Delta U_0 \delta_{\omega,0}}{\mu_R} \tag{17}$$

ρ_1 and ρ_2 are the densities of the two different layers of the shear flow, ΔU_0 is the initial velocity difference across the layer ($\Delta U_0 = U_1 - U_2$) and $\delta_{\omega,0}$ is the initial vorticity thickness ($\delta_{\omega,0} = 0.006859$ m).

6. Initial and boundary conditions

We chose the configuration of a temporal oxygen/hydrogen mixing layer investigated by Okong'o et al. [3] as a validation test case. The domain is periodic in x_1- and x_3-direction and of outflow type in the x_2-direction. The layer is not symmetric in x_2 as the layer growth is expected to be significantly larger on the hydrogen side. Tab. (1) summarizes the the mixing layer's mean flow properties. The free stream densities (ρ_1 and ρ_2) are calculated at the free stream temper-

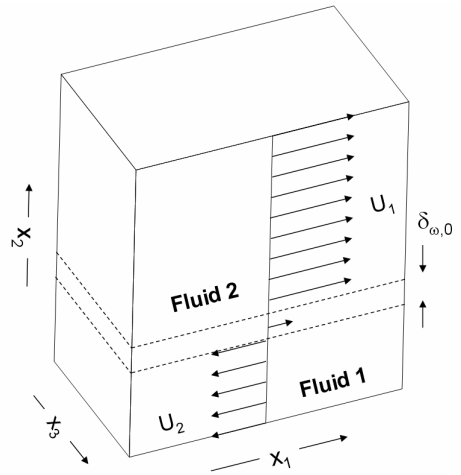

Figure 1: Mixing layer configuration: fluid 2 = hydrogen, fluid 1 = oxygen.

atures (T_1 and T_2) and the initial uniform pressure p_0 using the specified EOS. The initial mean profiles for streamwise velocity, temperature and species mass fractions are prescribed using an error function profile $\mathrm{erf}\left(\sqrt{\pi} x_2 / \delta_{\omega,0}\right)$. To initiate the layer roll up, vorticity disturbances are superimposed on the mean velocity profile. The wave length for these disturbances corresponds to the most unstable incompressible mode [11]. These streamwise and spanwise disturbances are specified as:

$$\omega_1 \left(x_2, x_3\right) = F_{3D} \frac{\lambda_1 \Delta U_0}{\Gamma_1} f_2 \left(x_2\right) f_3 \left(x_3\right) \tag{18}$$

$$\omega_3 \left(x_1, x_2\right) = -F_{2D} \frac{\lambda_3 \Delta U_0}{\Gamma_3} f_1 \left(x_1\right) f_2 \left(x_2\right) \tag{19}$$

The functions f_1, f_2 and f_3 are are given by

$$f_1 \left(x_1\right) = \sum_{i=0}^{2} A_i \left| \sin\left(\frac{\pi x_1}{2^i \lambda_1}\right) \right| + A_3 \left| \sin\left(\frac{\pi x_1}{8\lambda_1} - \frac{\pi}{2}\right) \right| \tag{20}$$

Table 1: Mixing layer mean flow properties.

Mean quantity	$x_2 = -\infty$ (O_2)	$x_2 = \infty$ (H_2)
$\bar{u}_1$, m/s	-158.004	770.983
$\bar{\rho}$, kg/m^3	96.764	3.965
p_0, atm	100	100
T, K	400	600
Y_O	1	0

Table 2: Domain size and grid resolutions for H2/O2 mixing layer.

Cases	Domain size $L_1 \times L_2 \times L_3$,m^3	Grid resolution $N_1 \times N_2 \times N_3$
DNS	0.2×0.2×0.12	352×352×208
LES	0.2×0.2×0.12	88×88×52

$$f_2(x_2) = \exp\left[-\pi\left(\frac{x_2}{\delta_{\omega,0}}\right)^2\right] \tag{21}$$

$$f_3(x_3) = B_0 \sin\left(\frac{2\pi x_3}{\lambda_3}\right) + B_1 \sin\left(\frac{\pi x_3}{L_3}\right) \tag{22}$$

The relative amplitudes of the vorticity disturbances are chosen to be $F_{2D} = 0.1$ and $F_{3D} = 0.05$. The the coefficients A_i and B_i have been given the values $A_0 = 1$, $A_1 = 0.5$, $A_2 = A_3 = 0.35$, $B_0 = 1$ and $B_1 = 0.025$. The perturbation wave length is $\lambda_1 = 7.29\delta_{\omega,0}$ and $\lambda_3 = 0.6\lambda_1$, corresponding to the domain size which is chosen to cover four wavelengths in streamwise and spanwise direction. Table (2) summarizes the investigated domain sizes and grid resolutions. The circulations Γ_1 and Γ_3 have to be calculated by integrating $f_2 f_3$ and $f_1 f_2$ over the respective planes and dividing by twice the number of wavelengths in x_1 and once the number of wavelengths in x_3, respectively (Eqns. (23) - (24)).

$$\Gamma_1 = \int\int \frac{\left|f_y f_z\right| \Delta_y \Delta_z}{2 \cdot 4} \mathrm{d}y\mathrm{d}z \tag{23}$$

$$\Gamma_3 = \int\int \frac{\left|-f_x f_y\right| \Delta_x \Delta_y}{1 \cdot 4} \mathrm{d}x\mathrm{d}y \tag{24}$$

The initial velocity fluctuations can then finally be determined by solving the corresponding Poisson equations for the vorticities. Tab. 2 summarizes the investigated domain sizes and grid resolutions for the DNS and LES.

7. Results

In this section we compare the results of our reference DNS with ALDM, OEM and DOEM. Of course, an LES cannot recover all the features of a much higher resolved DNS by definition. Therefore, the DNS results must be filtered and coarsened to the LES grid resolution for comparison with the LES results. We obtain the filtered DNS (FDNS) as reference solution by top-hat filtering over cubes of 4x4x4 cells.

7.1 Global quantities

The time evolution of the global quantities of a mixing layer is a good measure for its global characteristics. It gives for example information whether small-scale vortex formation is supported which causes the mixing layer to reaches

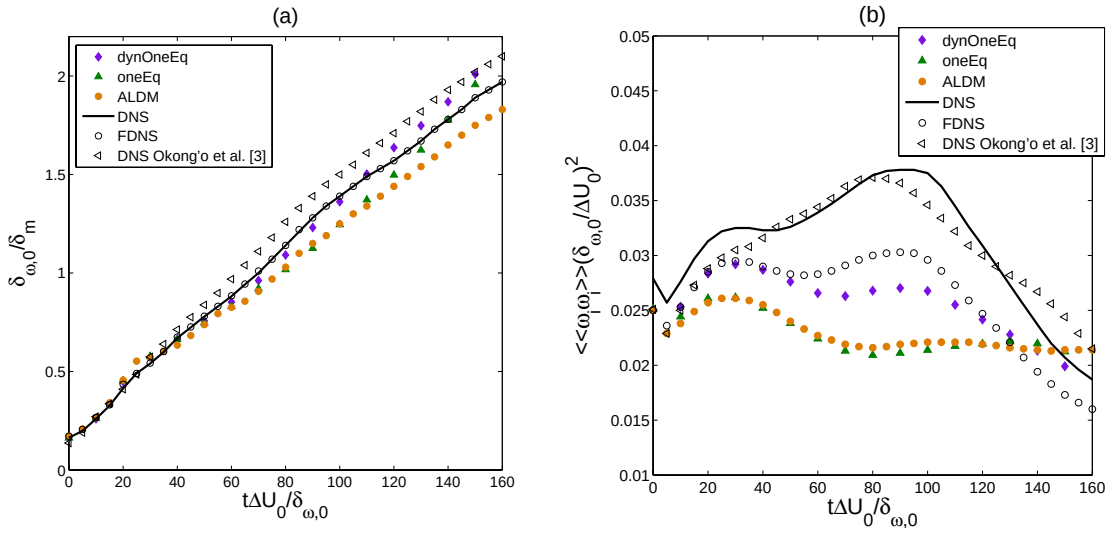

Figure 2: Time evolution of the mixing layer's nondimensional momentum thickness $\delta_m/\delta_{\omega,0}$ (a) and enstrophy $\langle\langle\omega_i\omega_i\rangle\rangle\,(\delta_{\omega,0}/\Delta U_0)^2$ (b).

transition. In the following, we compare the momentum thickness δ_m (Eqn. (25)) and the volume-averaged enstrophy $\langle\langle\omega_i\omega_i\rangle\rangle$ from our LES runs and the results of the FDNS. While the momentum thickness is a measure for the overall growth of the mixing layer, the volume-averaged enstrophy gives information about stretching and tilting inside the layer, both of which being responsible for vorticity production and the formation of small scales and thus being a measure for turbulence.

$$\delta_m = \frac{\int_{x_2,min}^{x_2,max}\left[\langle\rho u_1\rangle_{x_2,max} - \langle\rho u_1\rangle\right]\left[\langle\rho_1\rangle - \langle\rho u_1\rangle_{x_2,min}\right]\mathrm{d}x_2}{(\langle\rho u_1\rangle_{x_2,max} - \langle\rho u_1\rangle_{x_2,min})^2} \tag{25}$$

Fig. 2 (a) shows the time evolution of the non-dimensional momentum thickness. Filtering does not significantly alter the values in this case, therefore the FDNS results do not differ from the original DNS. For comparison also the DNS results of Okong'o et al. [3] have been ploted. The DNS performed at TUM predicts a slightly smaller layer growth, which might be caused by differences in the determination of the initial conditions and the applied numerics. As the simulations in OpenFOAM and the INCA code have been kept as similar as possible in initialisation and discretisation, the results of these two codes will be validated against each other further on.
All tested models capture the mixing layer growth very well. ALDM slightly underestimates the layer groth. The OEM shows some small deviations from the DNS results around the time of the first pairing of the vortices at $t^* = t\Delta U_0/\delta_{\omega,0} = 80$. At the time of the second pairing ($t^* = 150$, also the transitional time) it matches the momentum thickness of the FDNS very well. The DOEM fits the DNS data over almost the whole simulation period and only overestimates the mixing layer growth sightly after $t^* = 120$.
The time evolution of the non-dimensional enstrophy is shown in Fig. 2 (b). The trend of the DNS values agrees very well with the results from [3], demonstrating that we are generally able to reproduce the fundamental characteristics of the reference test case. Filtering the DNS solution removes the small scale fluctuations, leading to a lower overall enstrophy distribution of the FDNS. The present calibration of ALDM for ideal gases and the non-dynamic OEM are obviously too dissipative to recover the formation of small scale structures to its full extent. The DOEM fits the FNDS results in the beginning of the simulation and underestimates the enstrophy between $t^* = 50$ and $t^* = 130$. Later the enstrophy is slightly overpredicted. This model is able to reproduce the fundamental characteristics of the enstrophy time evolution, although it is too dissipative in general. Nevertheless, DOEM does not smear all the small structures and is still able to follow the periodic growth and shrinkage of the enstrophy which is caused by the rollup of the mixing layer. In general it could be shown that OpenFOAM and INCA are well-suited for this kind of test case and provide reasonable results.

7.2 Visualizations of the flow

Instantaneous visualizations of the flow support the findings derived from the global quantities. Fig. 3 (right) shows the oxygen mass fraction and the non-dimensional streamwise vorticity in the x_2-x_3-plane at $x_1 = 0.1756$ m. Shape, magnitude and position of the upper vortices obtained with all models agree very well with the FDNS results. ALDM and OEM underestimate the negative peak values, which are fit very well with the DOEM. The lower vortices are too small for OEM and ALDM, probably due to too much dissipation created by the SGS model, which perfectly meets the characteristics of the global enstrophy, whereas the DOEM also reproduces these vortex positions.
The O_2 mass fraction in the x_2-x_3-plane at $x_1 = 0.1756$ m (Fig. 3 (left)) gives a similar result. Here all models come very close to the shape of the FDNS result, only the shape of the structures is less distorted. The oxygen distribution given by the DOEM is also closest to the FDNS data.
The results for the non-dimensional spanwise vorticity (Fig. 4 (right)) in the x_1-x_2-plane at $x_3 = 0.06$ m show comparable behaviour. DOEM is able to reproduce many of the geometrical features of the FDNS contour as well as the overall position. The magnitude is generally in the right range as well. Although having a similar shape, the position of the ALDM and OEM results is shifted somewhat to the left. The results obtained with OpenFOAM do not match the shape of the high vorticity region in the lower part of the flow field, which is probably caused by boundary interactions.

Regions with so-called high density gradient magnitude (HDGM) are of special interest among the geometrical features of the mixing layer. They redistribute turbulent energy from the normal to the tangential direction [12], therefore being crucial for the correct simulation of mixing and combustion. As can be seen in Fig. 4 (middle), again all models are able to reproduce the most important geometrical features of the FDNS solution's density gradient. Although the peak values do not fully match, the shape and position of many small structures computed agree very well with the FDNS result.

The results for the O_2 mass fraction in the x_1-x_2-plane at $x_3 = 0.06$ m (Fig. 4 (left)) are slightly different from the previous findings. The shapes of the vortex computed with ALDM and OEM are quite smooth, indicating a substantial amount of dissipation during the simulation. The general flow characteristics are met well. Geometrical features are more smeared out in the LES, e. g. hydrogen implications in the oxygen stream like they occur in the FDNS can't be reproduced by the LES. These phenomena can also hardly be reproduced with DOEM, but it fits the overall shape of the O_2 distribution best.

8. Conclusions and outlook

We simulated a non-reacting, transitional, temporal mixing layer of counter-flowing hydrogen and oxygen by means of the ILES method ALDM and an LES with OEM and DOEM. Additionally, a DNS of the configuration was simulated as a reference for comparison with the LES results.

ALDM and OEM show a good agreement with the FDNS results in the instantaneous flow visualizations. They capture already the most important geometrical flow features with their current parameterization. The global quantities however show, that both models are too dissipative for the full reproduction of the FDNS results. DOEM provided the best agreement with the FDNS results in the instantaneous flow visualisations and has also been able to reproduce the transient global quantities very well.

INCA could show its capability of performing high quality real gas simulations (DNS and LES). These will yield the basis for a further improvement of ALDM for real gas flow and thereby for the very detailed investigation of supercritical flow phenomena.

With the presented investigations, OpenFOAM qualifies as a promising tool for the final goal of simulating reacting flows in a rocket combustion chamber.

Future work will therefore focus on optimization of the SGS modelling for real gas flows and later on the simulation of supercritical jet injections. As the next step it is planned to investigate an additional configuration of counter-flowing heptane and nitrogen, which will be used for further validation. Here results of different SGS models are already available for comparison [12].

Acknowledgments

Financial support has been provided by the German Research Foundation (Deutsche Forschungsgemeinschaft – DFG) in the framework of the Sonderforschungsbereich Transregio 40. Computational resources have been provided by the Leibniz-Rechenzentrum München (LRZ).

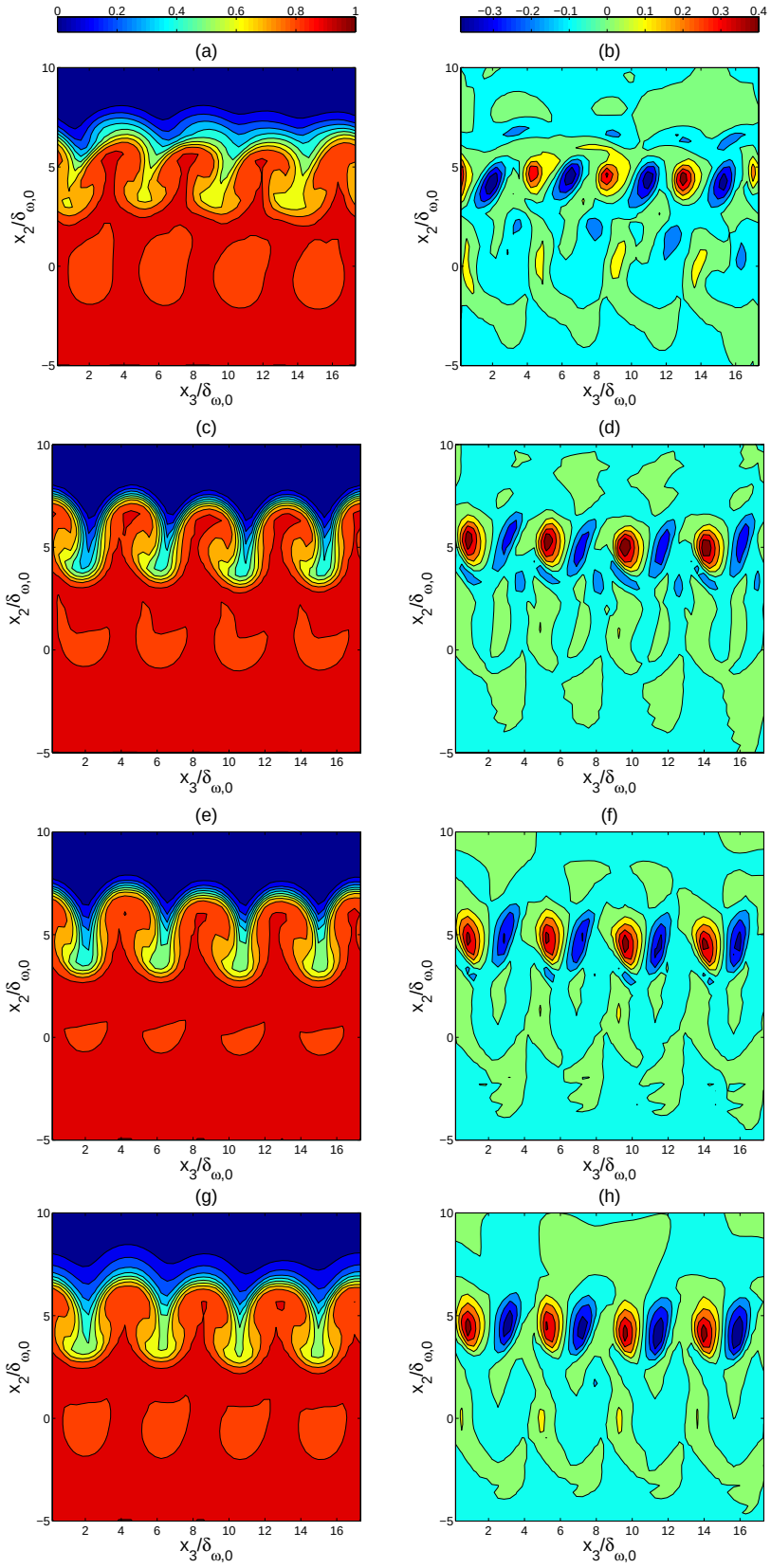

Figure 3: Y_O for (a) FDNS, (c) ALDM, (e) OEM and (g) DOEM and $\omega_1\delta_{\omega,0}/\Delta U_0$ for (b) FDNS, (d) ALDM, (f) OEM and (h) DOEM at $t^* = 150$ in the x_2-x_3-plane at $x_1 = 0.1756$ m.

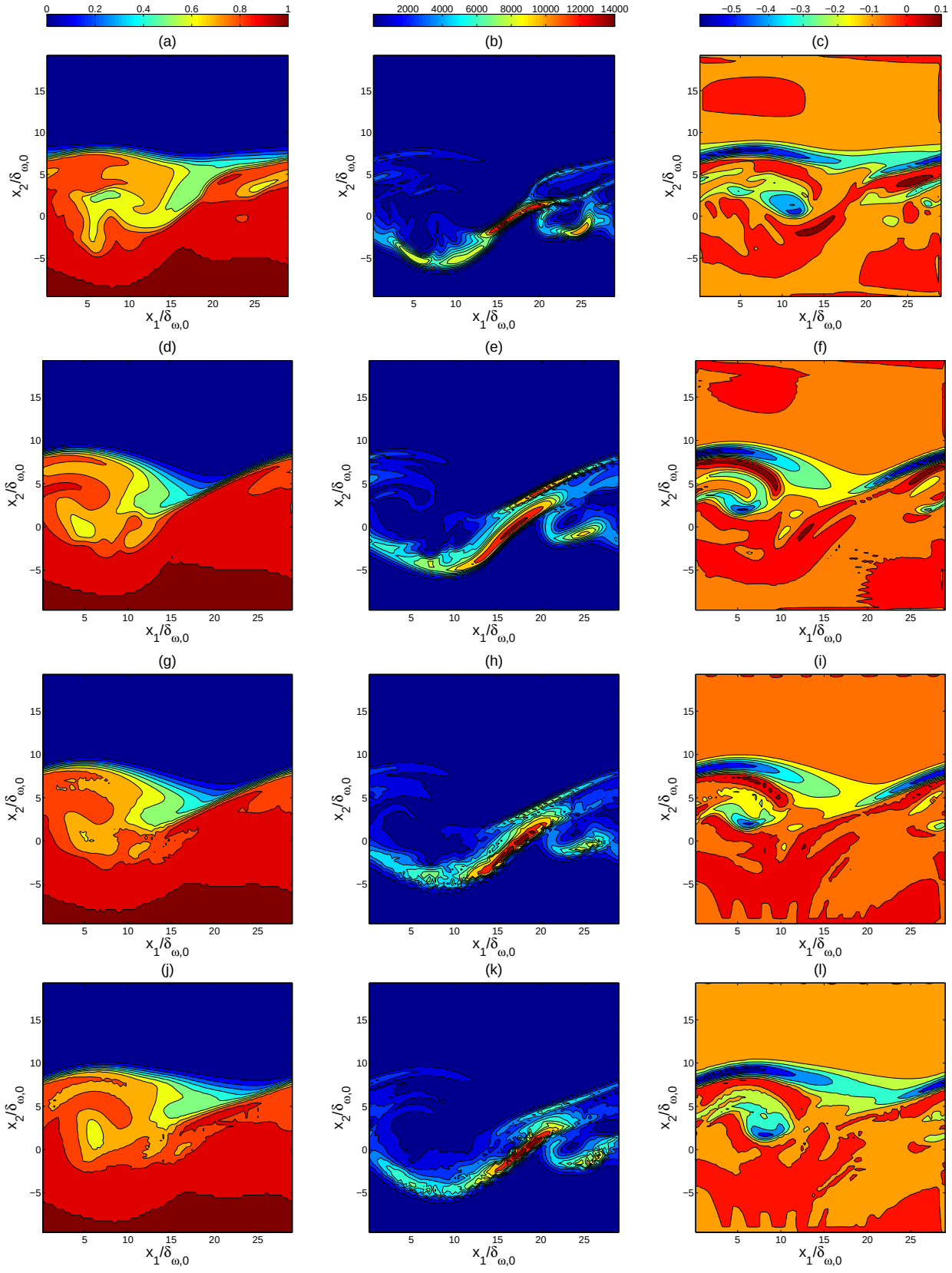

Figure 4: Y_O for (a) FDNS, (d) ALDM, (g) OEM and (j) DOEM, $|\nabla\rho|$ in kg/m^4 for (b) FDNS, (e) ALDM, (h) OEM and (k) DOEM and $\omega_3\delta_{\omega,0}/\Delta U_0$ for (c) FDNS, (f) ALDM, (i) OEM and (l) DOEM at $t^* = 150$ in the x_1-x_2-plane at $x_3 = 0.06$ m.

References

[1] Peng D.-Y. & Robinson D. P. (1976). A New Two-Constant Equation of State In: *Ind. Eng. Chem. Fundam.*, 15(1):59–64.

[2] Harstad K., Miller R. & Bellan J. (1997). Efficient High-Pressure State Equations. In: *AIChE Journal*, 43(6):1605–1610.

[3] Okong'o N., Harstad K. & Bellan J. (2002). Direct Numerical Simulations of O_2/H_2 Temporal Mixing Layers Under Supercritical Conditions. In: *AIAA Journal*, 40(5): 914–926.

[4] Hickel, S. & Larsson, J. (2008). An adaptive local deconvolution model for compressible turbulence. In: *Proceedings of the CTR Summer Program 2008*, 85–96.

[5] Hickel, S. & Larsson, J. (2011). Implicit subgrid-scale modeling for LES of shockwave turbulence interaction. In: *In preparation*.

[6] Sarman S. & Evans D. (1992). Heat flux and mass diffusion in binary Lennard-Jones mixtures. In: *Phys. Review A: General Physics*, 45(4):2370–2379.

[7] Miller, R., K. Harstad & J. Bellan. 2001. Direct numerical simulations of supercritical fluid mixing layers applied to heptane-nitrogen. In: *J. Fluid Mech.*. 436:1–39.

[8] Issa R. (1985). Solution of the Implicitly Discretised Fluid Flow Equations by Operator-Splitting. In: *J. Comp. Phys.*, 62:40–65.

[9] Issa R., Ahmadi-Befrui B., Beshay K. & Grosman A. (1991). Solution of the Implicitly Discretised Reacting Flow Equations by Operator Splitting. In: *J. Comp. Phys.*, 93:388–410.

[10] Schumann U. (1975). Linear stability of finite difference equations for three-dimensional flow problems. In: *J. Comp. Phys.*, 18:465–470.

[11] Moser R. & Rogers M. (1991). Mixing transition and the cascade to small scales in a plane mixing layer In: *Phys. Fluids A*, 3:1128–1134.

[12] Taskinoglu E. & Bellan J. (2010). A posteriori study using a DNS database describing fluid disintegration and binary-species mixing under supercritical pressure: heptane and nitrogen In: *J. Fluid Mech.*, 645:211–254.